Combustion Modeling Study for a GCH4/GOX single element combustion chamber: Steady State Simulation and Validations

By Yu Daimon, H. Terashima†, H. Negishi AND O. Haidn‡
Japan Aerospace Exploration Agency, 2-1-1 Sengen, Tsukuba, Ibaraki, Japan

1. Introduction

Oxygen/methane is a very attractive propellant combination for the rocket propulsion of spacecraft because it provides a specific impulse improvement of several dozen seconds compared with storable propellants. The LOX/LCH$_4$ combination may be said to be "space storable" (liquid temperature is 90 K-130 K depending on tank pressure). With passive thermal protection, boiling rates of methane are significantly lower than those of hydrogen. Another significant advantage is the absence of human health risks. Therefore, the investigations of this research field in recent decades have focused on the application of methane for propulsion in space [1-3]. Improving our knowledge of heat transfer processes and cooling methods in the combustion chamber is crucial to develop high-performance liquid rocket engines.

Within this framework, an experimental test campaign was performed at TUM on a gaseous oxygen (GOX)/gaseous methane (GCH$_4$) shear coaxial single-element injector, and wall heat transfer characteristics were discussed. Numerically, steady state and unsteady simulations were performed. The steady state simulation for Reynolds-averaged Navier-Stokes simulations (RANS) was used to reproduce the combustion pressure and wall heat flux distributions, and the results were compared with experimental data. In addition, the different combustion models were compared with each other to improve the understanding of the heat transfer and flame structure. The focus of the unsteady simulation was the flame structure near the face plate. The unsteady simulation results are provided in a separate report. To accurately predict heat transfer properties in an actual thrust chamber of a specific size, a simulation tool based on RANS is a prerequisite from an engineering perspective. The simulation code in this study was validated by a comparison with experimental heat flux data in actual H$_2$/O$_2$ thrust chambers with single and multi-injections [4-6]. This simulation code was applied to a combustion simulation of the GOX/GCH$_4$ coaxial single-element injector.

2. Experimental and Numerical Setup

2.1. *Experimental Setup*

The test campaign described in this study was performed at TUM [7]. A single-element injector combustion chamber was used, featuring the same injector design and chamber

† University of Tokyo, 2-11-16 Yayoi, Bunkyo, Tokyo, Japan
‡ Lehrstuhl für Flugantriebe, Professur für Raumfahrtantriebe, Technische Universität München Boltzmannstr. 15, 85748 Garching b. München, Germany

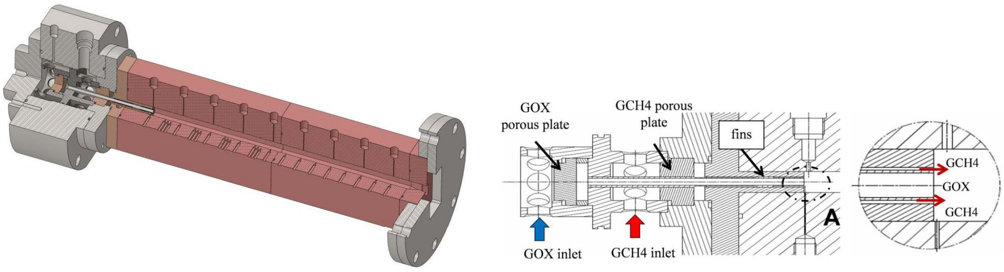

FIGURE 1. Single-element injector combustion chamber and details of injector configurations

O/F	Mass flow rate of O_2	Mass flow rate of CH_4	Temperature of O_2	Temperature of CH_4
-	[kg/s]	[kg/s]	[K]	[K]
2.65	0.045	0.017	278	269

TABLE 1. Inlet conditions.

contraction ratio as those of experimental multi-injector combustion chambers, to understand the injector-wall interaction. The combustion chamber has a 12 mm side cross section and a length, up to the throat, of 303 mm. Figure 1 shows the configuration of the single-element injector combustion chamber. Table 1 shows injection conditions for the static firing test. These parameters were used as boundary conditions for the numerical simulation.

2.2. *Computational Setup*

The numerical simulations in this study were performed using the density-based solver CRUNCH CFD, which was developed by Combustion Research and Flow Technology (CRAFT Tech) [8]. CRUNCH CFD is an unstructured/multi-element flow solver based on a cell-vertex method [9, 10]. The governing equations are the three-dimensional (3D) compressible Favre-averaged Navier-Stokes equations. Inviscid fluxes are calculated using a second-order linear reconstruction procedure based on a total variable diminishing scheme. Viscous fluxes are computed by estimating gradients at cell faces. The standard high Reynolds number k-ϵ and k-ω SST turbulence models [11] are used. The near-wall treatments of k-e model are based on the damping function [12] and the two layer model [13]. For time integration, an implicit solution procedure is employed, allowing for Gauss-Seidel or generalized minimal residual solver options with a preconditioning matrix using a distance-one neighbor bandwidth [10]. For the combustion model, laminar finite rate model with a skeletal chemical reaction set of CH_4/O_2 proposed by DLR is used. This model includes 21 species and 97 chemical reactions. As more attractive method for the computational cost, flamelet model is selected. To understand the difference between the laminar finite rate model and flamelet model, the simplest option which is laminar equilibrium chemistry is chosen. The result using the flamelet model was compared with that using the laminar finite rate model.

Figure 2 shows the 3D computational domain with boundary conditions. Moreover the figure shows the magnified views of the computational grid for several regions. In this case, a symmetry condition is assumed in the circumferential direction, and only a

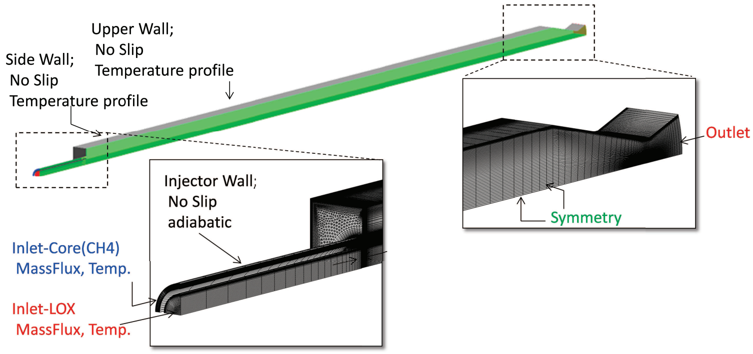

FIGURE 2. Computational grid and boundary conditions for the square thrust chamber with a single-element injector

quarter of the chamber is simulated. The number of computational grid points is approximately 3 million, in which the y^+ of the near-wall grid is about 0.1 along the entire region and 15 grid points are used on the GOX post. Grid resolution studies are performed to satisfy grid convergence for the wall heat flux using 2, 3, and 5 million grid points. The computational grid with 3 million grid points is used in this report. For boundary conditions, the supersonic outflow condition is imposed on the nozzle outlet, and the mass flow rate and static temperature of CH_4 and O_2 are specified at inlet boundaries for each fluid, as shown in Table 1, and thus, the chamber pressure obtained by the computation can be compared with the experimental value. A no-slip and isothermal wall with a temperature distribution estimated from the experiment is applied to the thrust chamber wall. For the other walls, no-slip and adiabatic conditions are imposed.

3. Results

3.1. *Validations*

In this section, comparisons between the simulation results and experimental data are presented. The *k*-ϵ turbulence model with the two-layer model [13] and the laminar finite rate model were selected for the comparison as turbulence and a combustion models, respectively. Figure 3 shows a comparison of pressure profiles on the chamber wall between the experimental data and simulation results, as well as the temperature distribution in the thrust chamber. The experimental data shows a steep rise from point 1 and 2 near the face plate and then a gradual decrease. The final two points at the end of the chamber show the same pressure level. These characteristics of the pressure distribution can be explained using the temperature distribution in the thrust chamber. The steep rise of the pressure distribution corresponds to the low temperature region at the corner, where recirculation occurs. The diffusion flame starts from the GOX post. The high temperature region, which corresponds to the diffusion flame, extends gradually. On the other hand, the low temperature region, which corresponds to the GOX core, narrows gradually. Moreover, combustion in the diffusion flame gradually induces a pressure drop along the axis. Therefore, because the final two points in the experimental data have the same pressure level, it can be inferred that combustion has already done. In the simulation results, the pressure does not show a flat profile at the end of the combustion chamber. This means that the GOX core length in the experiment is shorter than that in the simulation. In addition, the combustion pressure in the simulation result

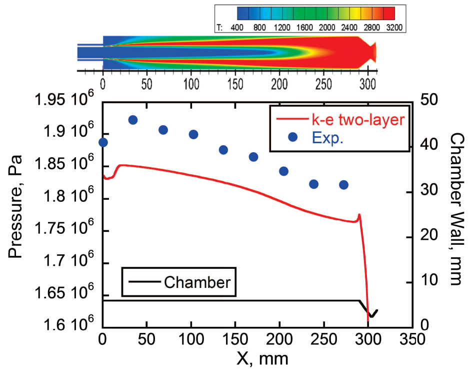

FIGURE 3. Temperature distribution and pressure profiles on the wall for the experimental data and simulation results

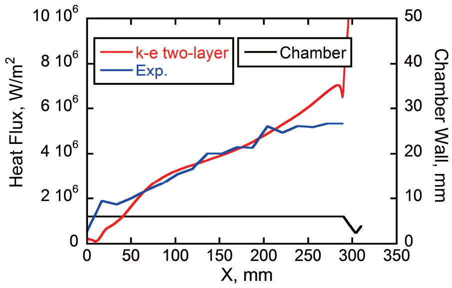

FIGURE 4. Heat flux profiles for the experimental data and simulation results

is 2.75 % lower than that in the experimental data. This tendency is consistent with the prediction of the GOX core length.

Figure 4 compares the heat flux distributions along the center line of the chamber wall for the experimental data and simulation results. The simulation results underestimate the value near the faceplate and overestimate it at the end of the combustion chamber. In the middle of the combustion chamber, the simulation results recreate the experimental data very well. The total wall heat flux of the simulation results is 2% higher than that of the experimental data. This tendency is consistent with the prediction for the combustion pressure. Based on the above discussion, it appears that there is a shortage of heat release near the face plate. To improve heat flux estimation near the face plate, the mixing between GCH_4 and GOX in that region is important. Increasing heat release near the face plate induces a shorter GOX core and flattens the heat flux distribution at the end of the combustion chamber.

3.2. *Effects of turbulence and combustion models*

In this section, using the simulation results for the GCH_4/GO_2 single-element injector, the effects of the turbulence and combustion models are discussed. Figure 5 shows the temperature distributions in the thrust chamber and the pressure profiles of the simulation results using k-ϵ with the near-wall treatments [12], k-ϵ with the two-layer model [13], and k-ω SST [11]. The temperature distributions between k-ϵ with the near-wall treatment and k-ϵ with the two-layer model are almost identical. This is because the damping function only affects the flow field near the wall. On the other hand, turbulence models, such as k-ϵ and k-ω in this study, have an effect on temperature distributions. The low temperature region on the center line, which indicates the GOX core, reaches the throat position in the results for k-ω SST. The combustion pressure levels are different but the shapes of the pressure distributions are almost identical qualitatively, e.g., the steep rise near the face plate and then a gradual decrease. The combustion pressure of k-ϵ with the two-layer model is slightly higher than that of k-ϵ with the near-wall treatment. This difference is discussed with the heat flux distribution shown in Fig. 6. The combustion pressure of k-ω SST is the lowest among the three turbulence models. In other words, the combustion efficiency in the result for k-ω SST is lower than that for k-ϵ because

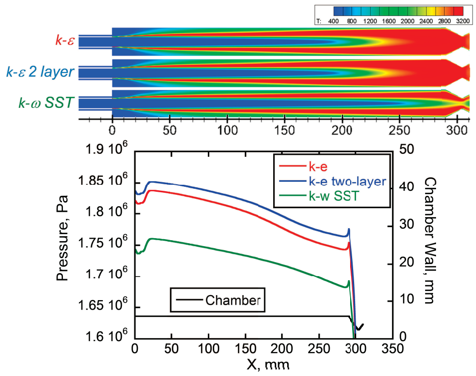

FIGURE 5. Temperature distributions and pressure profiles

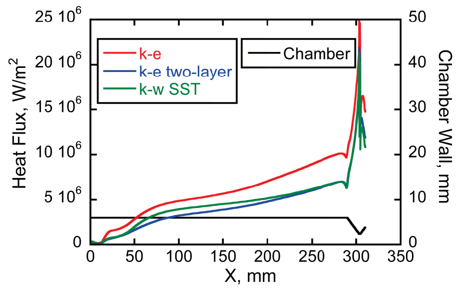

FIGURE 6. Wall heat flux distributions along the center line of the combustion chamber

combustion does not finish at the end of the chamber, as shown in the temperature distribution.

Figure 6 shows the wall heat flux distributions of the simulation results using k-ϵ with the near-wall treatments [12], k-ϵ with the two-layer model [13], and k-ω SST [11]. The effect of the damping function can be observed in the heat flux distributions. The heat flux of k-ϵ with the near-wall treatment is higher than that of k-ϵ with the two-layer model. On the other hand, the pressure difference between *k*-*e* with the near-wall treatment and *k*-*e* with the two-layer model is relatively small, and temperature contours are almost identical as shown in Fig 5. Therefore, this difference in the heat flux arises from an effect of the damping function. The heat flux of k-ω SST is lower than that of k-ϵ with the near-wall treatment. As shown in Fig. 5, the pressure and combustion efficiency of k-ω SST are lower than those of k-ϵ with the near-wall treatment. Even if the pressure correction $\dot{q} \propto p_c^{0.44}$ proposed in a previous study [7] is applied to the heat flux of k-ω SST, the profile of the heat flux does not much that of k-ϵ with the two-layer model. Therefore, this difference in the heat flux is not caused by the pressure effect but by the effect of the turbulence models in the thermal boundary layer.

The laminar finite rate combustion model needs the same number of equations as included species. On the other hand, the flamelet model needs just two equations. The computational time required for using the laminar finite rate combustion model is seven times higher than that required for using the flamelet model in CRUNCH CFD with the methane chemical reaction set proposed by DLR. The flamelet model is a very attractive combustion model from the view point of computational cost. In this section, we discuss problems with the flamelet model. CRUNCH CFD [8] has several flamelet model options. To understand differences between the laminar finite rate combustion model and flamelet model, the simplest flamelet option, i.e., the laminar equilibrium chemistry option, was selected. Figure 7 shows the temperature distributions and pressure profiles of the simulation results using the laminar finite rate model and flamelet model with laminar equilibrium chemistry. The turbulence model in the both cases is k-ϵ with the near-wall treatment. The temperature distributions are almost identical in the combustion chamber. It means that the reaction rate is very fast and that the diffusion of chemical species determines the flow field. In the nozzle part, the temperature of the flamelet model is lower than that of the laminar finite rate model. The flamelet model does not consider the pressure effect in the flamelet table. Therefore, chemical compositions at the throat

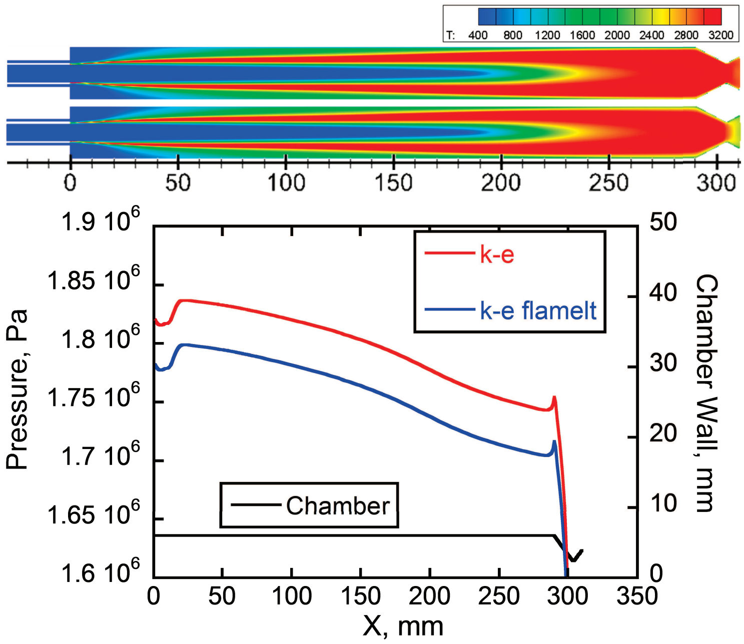

FIGURE 7. Temperature distributions and pressure profiles

are different between the two models. This effect appears in the combustion pressure. The combustion pressure obtained using the flamelet model is lower than that using the laminar finite rate model.

Figure 8 shows the wall heat flux distributions of the simulation results using the laminar finite rate model and flamelet model with laminar equilibrium chemistry. The heat flux distributions are almost identical in the range $0 < x < 200$ mm. Beyond 200 mm, the wall heat flux of the simulation results using the flamelet with laminar equilibrium chemistry is lower than that using the laminar finite rate model. As shown in Figure 7, the temperature distributions are almost identical in the combustion chamber. There is no specific characteristic around 200 mm that affects the temperature distributions. Therefore, the difference in the heat fluxes between the laminar finite rate model and flamelet model appears in a very thin thermal boundary layer on the chamber wall. In general, the species mass fractions should change because of the heat loss effect at the chamber wall. However, the table of this flamelet model was generated under adiabatic conditions. The heat loss effect in the combustion simulation appears in the species mass fraction on the wall. Figure 9 shows the CO_2 mass fraction distributions of the simulation results on the combustion chamber wall at the center using the laminar finite rate model and flamelet model with laminar equilibrium chemistry. The flamelet model underestimates the CO_2 mass fraction downstream of x = 200 mm, indicating the occurrence of recombination near the low temperature wall in the result of the laminar finite rate model, such as in CO_2 and H_2O. The diffusion flame has heat loss near the combustion chamber wall. The flamelet model cannot recreate the recombination due to such heat loss because the flamelet table does not assume the heat loss effect. Therefore, the flamelet model without the heat loss effect is not appropriate for wall heat flux estimation.

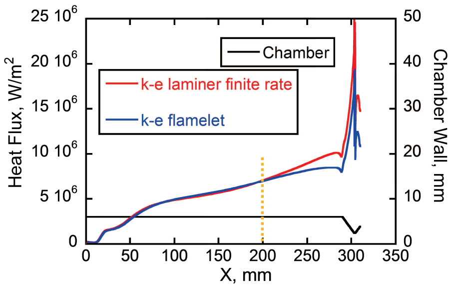

FIGURE 8. Wall heat flux distributions along the center line of the combustion chamber

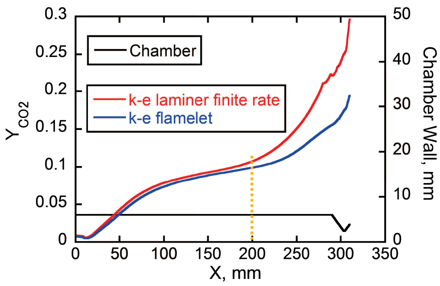

FIGURE 9. CO_2 mass fraction distributions along the centerline of the combustion chamber

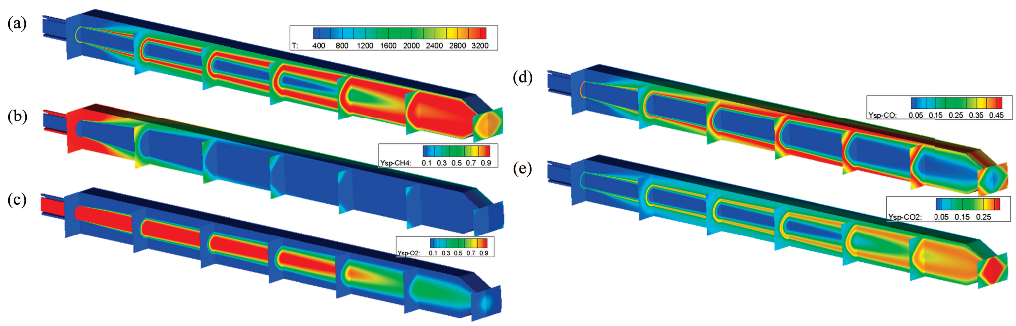

FIGURE 10. Contours in the cross sections of (a) temperature, (b) CH_4, (c) O_2, (d) CO, and (e) CO_2 mass fraction

3.3. *Three-dimensional characteristics of square chamber flow*

A characteristic of this test is the shape of the combustion chamber, which has a square cross section. In this square chamber, there are 3D characteristics that must be considered. These 3D properties are discussed in this section. Figure 10 shows the contours in the cross sections of (a) temperature, (b) CH_4, (c) O_2, (d) CO, and (e) CO_2. The high temperature region, which corresponds to the diffusion flame, is the round shape in the cross section near the face plate. In the downstream, this shape changes into that of diamond because of corner effects in the square chamber. There are low temperature regions at the corners of the combustion chamber shown in Fig. 10a. These low temperature regions include the unburned fuel, i.e., CH_4, as shown in Fig. 10b. This unburned fuel comes from the recirculation zone near the face plate, shown later. The low temperature region on the center line corresponds to the unburned oxidizer, i.e., O_2, as shown in Fig. 10c. This distribution in the cross sections also changes from a round to diamond shape further downstream. The CO mass fraction appears between CH_4 and CO_2, as shown in Fig. 10d and 10e. The products, such as CO_2, are generated on the flame. The distribution also takes a diamond shape at the nozzle exit.

Figure 11 shows (a) the contour of the wall heat flux and (b) its distributions in the circumferential direction at x = 25, 50, 100, 150, 200, and 250 mm. Note that the definition of the wall heat flux is negative in Fig. 11a. There is a distribution in the circumferential direction. The center line shows the highest wall heat flux in the circumferential

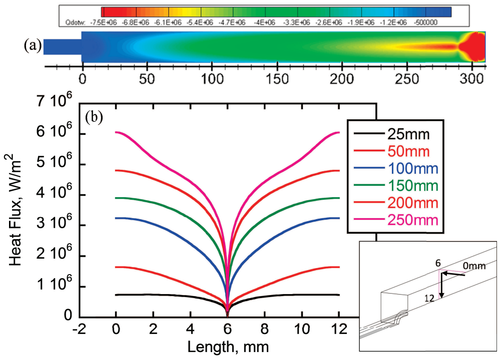

FIGURE 11. Contour of heat flux on the chamber wall and heat flux distributions in the circumferential direction

direction. The 0 and 6 mm points indicate the center line and corner of the combustion chamber wall, respectively. The wall heat flux at the corner is 0 MW/m^2. Therefore, the inclination at x = 250 mm is very large near the corner. In this frame work, the experiment and simulation results for the distribution in the circumferential direction cannot be compared. The simulation strongly demands the comparison of the wall heat flux in the circumferential direction with the experimental data.

Figure 12 shows stream lines near the face plate. Each figure corresponds to a different view; (a) bird's eye, (b) face plate, (c) upper wall, and (d) side wall. The color of the stream lines indicates the temperature of the flow field. The recirculation flow direction is a characteristic feature of this flow. The recirculation flow at the corner passes through the center line on the wall surface. This flow direction is the same as the injection flow. On the other hand, the direction of the recirculation flow on the wall of a round combustion chamber is opposite to that of the injection flow. If a film cooling flow is injected from the faceplate along the chamber wall, film cooling effects between the square and round combustion chambers will be different. In the square chamber, the film cooling flow will be accelerated by the recirculation flow, thereby increasing the film cooling efficiency.

4. Conclusions

3D RANS simulations were performed for the static firing test of a GOX/GCH_4 coaxial single-element injector with the square chamber, which was performed at TUM. The simulation code, CRUNCH CFD, was validated using the heat flux and pressure distributions, and showed good agreement with the experimental data overall. In detailed, the simulation results underestimate the value near the faceplate and overestimate it at the end of the combustion chamber. The combustion pressure in the simulation result was 2.75 % lower than that in the experimental data. All characteristics of these errors indicated that the mixing between GCH_4 and GO_2 was not sufficient in the simulation results. The comparison results indicated that the flame length in the experiment was shorter than that in the simulation. Using the simulation results for the GCH_4/GO_2 single-element injector, the effects of the turbulence and combustion models were discussed. The turbulence model and the damping function for the near-wall treatment had a big effect for the wall heat flux estimation. The problems of the flamelet model with laminar equilibrium chemistry were revealed. The flamelet model with laminar equilibrium chemistry of CRUNCH CFD does not consider the pressure and heat loss effects.

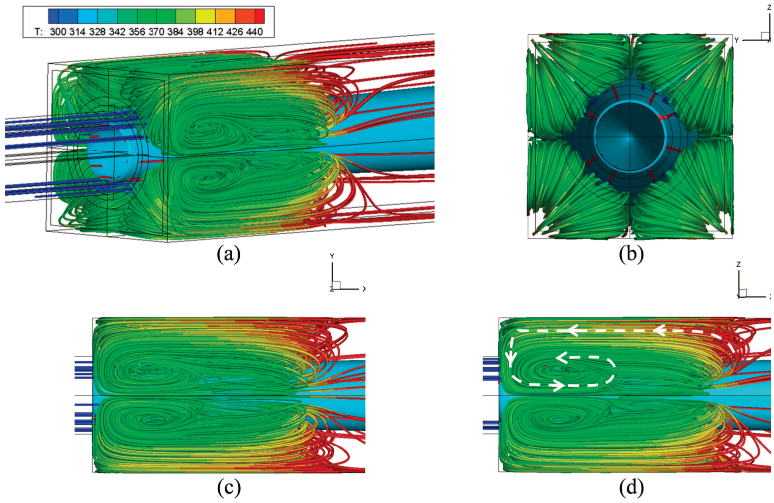

FIGURE 12. Figure 12 Stream lines near the face plate; (a) bird's eye view, (b) face plate view, (c) upper wall view, and (d) side wall view

Therefore, the changes of species mass fraction for the pressure drop in the nozzle and the recombination near the low temperature wall could not be recreate using the flamelet model. Finally, 3D characteristics of the combustion chamber with the square cross section were discussed. The distributions of species mass fraction and temperature showed the diamond shapes in the downstream region. The wall heat flux had the distribution in the circumferential direction. To understand the multi element injector flow field, these 3D characteristics should be validated as a next step.

Acknowledgments

Financial support has been provided by the German Research Foundation (Deutsche Forschungsgemeinschaft – DFG) in the framework of the Sonderforschungsbereich Transregio 40.

References

[1] TRINH H., "Liquid Methane/Oxygen Injector Study for Potential Future Mars Ascent Engines," AIAA 2000-3119, 36th AIAA/ASME/SAE/ASEE Joint Propulsion Conference and Exhibit, 17-19 July 2000

[2] CRAIG JUDD D., BUCCELLA S., ALKEMA M., HEWITT R., VEITH E., "Effect of Combustion Process on Performance, Stability, and Durability of a LOX/Methane Rocket Engine", AIAA 2006-1533, 44th AIAA Aerospace Sciences Meeting and Exhibit, 9- 12 January, 2006

[3] CRAIG JUDD D., BUCCELLA S., ALKEMA M., HEWITT R., MCLAUGHLIN B., HART G., VEITH E., Development Testing of a LOX/Methane Engine for In-Space Propulsion, AIAA 2006-5079, 42nd AIAA/ASME/SAE/ASEE Joint Propulsion Conference & Exhibit, 9-12 July 2006

[4] DAIMON, Y., NEGISHI, H, YAMANISHI, N., NUNOME, Y., SASAKI, M., AND TOMITA, T., "Combustion and Heat Transfer Modeling in Regeneratively Cooled

Thrust Chambers (Multi-Injection Flow Features)," 47th AIAA/ASME/SAE/ASEE Joint Propulsion Conference and Exhibit, AIAA Paper 2011-5625, July 31-August 03, 2011.

[5] DAIMON, Y., NEGISHI, H.M AND YAMANISHI, N., "Combustion and Heat Transfer Modeling in Regeneratively Cooled Thrust Chambers (Wall Heat Flux Validation)," 46th AIAA/ASME/SAE/ASEE Joint Propulsion Conference and Exhibit, AIAA Paper 2010-6723, July 25-28, 2010.

[6] DAIMON, Y., OHNISHI, Y., NEGISHI, H., AND YAMANISHI, N., "Combustion and Heat Transfer Modeling in Regeneratively Cooled Thrust Chambers (Co-axial Injector Flow Analysis)," 45th AIAA/ASME/SAE/ASEE Joint Propulsion Conference and Exhibit, AIAA Paper 2009-5492, August 2-5, 2009.

[7] SILVESTRI, S., CELANO, M. P., HAIDN, O., AND KNAV, O., "Comparison of Single Element Rocket Combustion Chambers with Round and Square Cross Sections," 6^{th} European conference for aeronautics and space sciences, 2015.

[8] URL: "https://www.craft-tech.com"

[9] HOSANGADI, A., LEE, R. A., YORK, B. J., SINHA N., AND DASH S. M., "Upwind Unstructured Scheme for Three-Dimensional Combustion Flows," *Journal of Propulsion and Power*, 12, 3, 494-503, 1996.

[10] HOSANGADI, A., ET AL., "Hybrid, Viscous, Unstructured Mesh Solver for Propulsive Applications," 34th AIAA/ASME/SAE/ASEE Joint Propulsion Conference and Exhibit, AIAA Paper 1998-3153, July 13-15, 1998.

[11] MENTER, F. R., "Two-Equation Eddy-Viscosity Turbulence Models for Engineering Applications," *AIAA Journal*, Vol. 32, No. 8, pp. 1598-1605, 1994.

[12] PAPP, J.L., AND DASH, S.M., "Turbulence Model Unification and Assessment for High-Speed Aeropropulsive Flows," Aerospace Sciences Meeting and Exhibit, 39th, Reno, NV, AIAA Paper 2001-880, January 8-11, 2001.

[13] WOLFSHTEIN, M., "The Velocity and Temperature Distribution in One-dimensional Flow with Turbulence Augmentation and Pressure Gradient," *Int J. Heat and Mass Transfer*, 12, pp.301-318, 1969.